Relativistic effects on ground state properties of 4d and 5d transition metals

1990 J. Phys.: Condens. Matter 2 4371

(http://iopscience.iop.org/0953-8984/2/19/006)

J. Phys.: Condens. Matter **2** (1990) 4371–4394. Printed in the UK

Relativistic effects on ground state properties of 4d and 5d transition metals

C Elsässer†‡, N Takeuchi†, K M Ho†, C T Chan†, P Braun‡ and M Fähnle‡

† Ames Laboratory, US Department of Energy and Department of Physics, Iowa State University, Ames, Iowa 50011, USA

‡ Max-Planck-Institut für Metallforschung, Institut für Physik, Heisenbergstrasse 1, 7000 Stuttgart 80, Federal Republic of Germany

Received 22 September 1989

Abstract. Cohesive energies, bulk moduli and equilibrium lattice constants have been calculated for the 4d and 5d transition metals with face-centred cubic crystal lattices (Rh, Pd, Ag and Ir, Pt, Au). For the total energy calculations according to the density functional theory in the local density approximation we have used an *ab initio* pseudopotential method. Two calculations have been performed for each element using either non-relativistic or scalar-relativistic ionic pseudopotentials. The pseudo-wavefunctions and charge densities of the valence electrons have been represented by a mixed basis of plane waves and localised orbitals derived from the atomic d pseudo-wavefunctions. For the 5d metals we find a significant improvement of the results by the relativistic treatment, as expected because of their heavy atomic nuclei. In the case of the 4d metals the relativistic results are of similar quality as for the 5d metals, but now the non-relativistic values are slightly closer to the experiment, possibly due to an error cancellation effect.

1. Introduction

One exciting topic in the solid state theory is the understanding and prediction of cohesive properties of transition metals and their alloys from first principles, without any experimental information being put into the calculation. A very successful theoretical framework for this is the density functional theory, initialised in the sixties by Hohenberg and Kohn (1964), in its local density approximation (LDA) (Kohn and Sham 1965). The progress in this theory is closely connected with the development of improved computers and efficient computer algorithms (for reviews see, e.g., Kohn and Vashishta 1983, Koelling 1981, Callaway and March 1984, Ihm 1988).

In the seventies self-consistent calculations became possible for cohesive properties of close-packed elemental metals, for example, with Slater's augmented-plane-wave method (APW) (Slater 1937) or the Green function method of Korringa, Kohn and Rostoker (KKR) (Korringa 1947, Kohn and Rostoker 1954). A collection of bulk and electronic properties for 32 metals from H to In, determined with the KKR method, has been published by Moruzzi, Janak and Williams (1978) and has become a kind of standard reference for density functional results.

0953-8984/90/194371 + 24 $03.50

The application of the APW and the KKR method is more or less limited to elemental solids by the following feature: the basis sets, augmented plane or spherical waves, respectively, are not independent of the energy and therefore lead to a non-standard eigenvalue problem with a complicated, non-linear energy dependence. This complication has been solved by linearisation of the energy dependence of the eigenvalue problem, yielding augmented basis orbitals which are independent of energy in the first order (Andersen 1975). Such linearised methods are for example the linear-muffin-tin-orbital method (LMTO) (Andersen 1975, Andersen 1984, Skriver 1984, Andersen *et al* 1985, Andersen *et al* 1987) or the closely related linear augmented-spherical-wave method (ASW) (Williams *et al* 1979). Both are developments of the KKR method which allow for calculations of systems with large and complicated unit cells. By making a shape approximation for the crystal potential, i.e. the potential is assumed to be spherically symmetric within touching muffin-tin spheres or slightly overlapping atomic Wigner–Seitz spheres around the atomic sites and flat in the remaining regions, the accuracy of the results decreases if the atoms are not close-packed. Calculations of lattice distortion energies are also problematic. However, this can be overcome by the full-potential LMTO method (Weyrich 1988, Methfessel 1988) or the FP LAPW method (Wimmer *et al* 1981, Weinert *et al* 1982).

Another method of calculation, using energy-independent basis sets and making no shape approximation, is provided by the pseudopotential theory which was developed during the sixties and seventies (Phillips and Kleinman 1959, Cohen and Heine 1970, Ihm *et al* 1979). Here only the valence electrons, which are responsible for the chemical binding, are treated explicitly whereas all the inert core electrons, together with the nuclei, are assumed to behave identically in the solid and in the free atoms. In this frozen-core approximation the influence of the core on the valence electrons is described by a pseudopotential. In earlier times this pseudopotential was usually an analytic model potential with several parameters which were chosen to reproduce some experimentally observed properties. The pseudopotential could also be derived from atomic core and valence wavefunctions without experimental information (Phillips and Kleinman 1959). In this scheme the pseudo-wavefunctions for atomic valence states have the same shape, but a different amplitude from the real wavefunctions outside the core region. This causes an error in the calculation of the Coulomb potential. Therefore it is a crucial problem in self-consistent calculations of electronic structures. With the use of norm-conserving *ab initio* pseudopotentials introduced by Hamann, Schlüter and Chiang (1979) these problems no longer exist and the pseudopotential method has become as *ab initio* as the above mentioned all-electron methods.

For many semiconductors (Yin and Cohen 1982) or simple metals (Lam and Cohen 1981) with only s and p valence states, the pseudopotentials are sufficiently smooth so that a small enough basis set of simple plane waves can be used. In the case of transition metals, the somewhat deeper pseudopotentials render plane-wave expansions uneconomical. A mixed basis consisting of plane waves and additional, well localised, energy-independent functions, which describe the more tightly bound nature of the d states, has proved to be very efficient (Louie *et al* 1979, Fu and Ho 1983).

By avoiding the explicit treatment of the large number of inert core electrons, this method is at least as effective as the all-electron methods. Because of the mathematically simple basis set, very fast computer algorithms like fast Fourier transformations and vectorisations yield a high calculational speed. No approximations are made for the shape of the potential. Besides the determination of total energies of equilibrium configurations it is possible to calculate energies of slightly or strongly distorted con-

figurations (e.g. phonon frequencies (Ho *et al* 1984), structural phase transitions (Yin and Cohen 1982, Chen *et al* 1988), surface reconstructions (Ho and Bohnen 1987)). Interatomic forces can be calculated (Ihm *et al* 1979, Ho *et al* 1983) using the Hellmann–Feynman theorem (Hellmann 1937, Feynman 1939). The approximations made, the neglect of the core charge density and the shape difference between real and pseudo-valence charge densities within a small sphere around the atomic positions, hold as long as the real core and valence charge densities do not significantly overlap outside this sphere.

The purpose of the investigations presented in this article is to assess the accuracy we can expect when using the density functional theory in LDA for the calculation of cohesive properties of composed systems containing transition metal elements, by comparing the results for single crystals with experimental values. In their aforementioned book Moruzzi *et al* (1978) published values for the 3d and 4d transition metals which are in very satisfactory agreement with experimental values. In their calculations they solved the Schrödinger equation for core and valence electrons. They did not take relativistic effects into account. This seems to be justified because the atomic nuclei were not too heavy. For 5d transition metals, on the other hand, the atomic nuclei are already so heavy that important influences of relativity, at least for the core electrons, are to be expected. To check these suppositions we have calculated the equilibrium lattice constants a_0, bulk moduli B_0 and cohesive energies E_0 for the series of face-centred cubic (FCC) crystals, Rh, Pd, Ag, and Ir, Pt, Au, on the right side of the 4d and 5d periods. Using an *ab initio* mixed-basis pseudopotential method (MB) with non-local pseudopotentials constructed both non-relativistically (NR) (Hamann *et al* 1979) and scalar-relativistically (SR), (with no spin–orbit coupling included) (Kleinman 1980, Bachelet and Schlüter 1982), we have calculated a_0, B_0, and E_0 for each crystal.

The article is organised as follows. In section 2 our calculation method is described. Several results about relativistic effects already appearing in the atomic calculations are mentioned. Section 3 contains our results for the solids which are compared with values from the experiment and previous calculations. An explanation of the differences between the non-relativistic and scalar-relativistic results, using band-structure and charge-density plots, is presented in section 4. In section 5 we give a summary of our results.

2. The mixed-basis pseudopotential method

2.1. Pseudopotentials

The generation of the non-local norm-conserving ionic pseudopotentials has been performed according to the prescription of Hamann *et al* (Hamann *et al* 1979, Bachelet and Schlüter 1982).

As a first step we have made atomic all-electron calculations for several different configurations of each atom within the LDA using the Hedin–Lundqvist parametrisation for the local exchange–correlation potential (Hedin and Lundqvist 1971). For both non-relativistic and fully relativistic calculations we have used a Herman–Skillman-type computer program (Herman and Skillman 1963). The pseudopotentials have been generated for prototype configurations by matching the non-relativistic or relativistic eigenvalues and nodeless pseudo-wavefunctions of the valence orbitals (4d, 5s, 5p and 5d, 6s, 6p, respectively, for the 4d and 5d metals) to the corresponding all-electron

eigenvalues and wavefunctions outside a core radius. In this scheme the relativistic effects on the valence electrons are incorporated in the pseudopotentials.

To test the transferability of the pseudopotentials we have made atomic pseudopotential and all-electron calculations for several configurations. In table 1 the valence orbital eigenvalues and the excitation energies for different configurations of Ag and Au obtained from the pseudopotential calculations are listed, and in brackets their deviations from the values of the all-electron calculations. The calculations for the other four elements exhibit similar deviations. In the relativistic case we give valence energy levels obtained without spin–orbit splitting (scalar-relativistic values (Bachelet and Schlüter 1982)). The non-relativistic and the scalar-relativistic levels of the 4d metals are only slightly changed, for the 5d metals occupied 6s and 6p levels are stronger shifted to lower energies, 5d levels to higher energies.

Table 1. (*a*) Non-relativistic atomic eigenvalues and excitation energies of silver (prototype configuration $[Kr]4d^{9.75}5s^{0.75}5p^{0.50}$). (*b*) Scalar-relativistic atomic eigenvalues and excitation energies of silver (prototype configuration $[Kr]4d^{9.75}5s^{0.75}5p^{0.50}$). (*c*) Non-relativistic atomic eigenvalues and excitation energies of gold (prototype configuration $[Xe]5d^{9.75}6s^{0.75}6p^{0.50}$). (*d*) Scalar-relativistic atomic eigenvalues and excitation energies of gold (prototype configuration $[Xe]5d^{9.75}6s^{0.75}6p^{0.50}$).

(*a*)	Valence state eigenvalues (Ryd)			Excitation
Configuration	d	s	p	energy (Ryd)
$[Kr]4d^{10}5s^{1}5p^{0}$	−0.6015	−0.3222	−0.0701	0
	(+0.0011)	(−0.0005)	(−0.0003)	(0)
$[Kr]4d^{10}5s^{0}5p^{1}$	−0.7317	−0.4100	−0.1387	0.2606
	(+0.0023)	(−0.0004)	(−0.0002)	(+0.0002)
$[Kr]4d^{9}5s^{2}5p^{0}$	−0.8717	−0.4067	−0.1126	0.3697
	(−0.0073)	(+0.0018)	(+0.0013)	(+0.0033)
$[Kr]4d^{9}5s^{1}5p^{1}$	−0.9905	−0.4837	−0.1717	0.6723
	(−0.0078)	(+0.0014)	(+0.0011)	(+0.0028)
$[Kr]4d^{9}5s^{0}5p^{2}$	−1.0928	−0.5464	−0.2168	0.9933
	(−0.0084)	(+0.0011)	(+0.0011)	(+0.0028)
$[Kr]4d^{10}5s^{0}5p^{0}$	−1.1887	−0.8047	−0.4640	0.5588
	(+0.0040)	(−0.0011)	(−0.0014)	(−0.0008)

(*b*)	Valence state eigenvalues (Ryd)			Excitation
Configuration	d	s	p	energy (Ryd)
$[Kr]4d^{10}5s^{1}5p^{0}$	−0.5691	−0.3524	−0.0678	0
	(+0.0013)	(−0.0003)	(0.0000)	(0)
$[Kr]4d^{10}5s^{0}5p^{1}$	−0.7082	−0.4495	−0.1421	0.2947
	(+0.0023)	(−0.0003)	(0.0000)	(+0.0003)
$[Kr]4d^{9}5s^{2}5p^{0}$	−0.8123	−0.4326	−0.1058	0.2959
	(−0.0057)	(+0.0019)	(+0.0017)	(+0.0026)
$[Kr]4d^{9}5s^{1}5p^{1}$	−0.9424	−0.5199	−0.1712	0.6331
	(−0.0066)	(+0.0012)	(+0.0014)	(+0.0025)
$[Kr]4d^{9}5s^{0}5p^{2}$	−1.0535	−0.5902	−0.2200	0.9927
	(−0.0075)	(+0.0009)	(+0.0014)	(+0.0028)
$[Kr]4d^{10}5s^{0}5p^{0}$	−1.1725	−0.8597	−0.4786	0.6010
	(+0.0040)	(−0.0011)	(−0.0011)	(−0.0007)

Table 1. (*continued*)

(*c*) Configuration	Valence state eigenvalues (Ryd) d	s	p	Excitation energy (Ryd)
$[Xe]5d^{10}6s^{1}6p^{0}$	−0.6140	−0.3320	−0.0752	0
	(+0.0008)	(−0.0004)	(−0.0002)	(0)
$[Xe]5d^{10}6s^{0}6p^{1}$	−0.7364	−0.4163	−0.1420	0.2645
	(+0.0017)	(−0.0003)	(−0.0002)	(+0.0001)
$[Xe]5d^{9}6s^{2}6p^{0}$	−0.8358	−0.4099	−0.1157	0.3525
	(−0.0048)	(+0.0015)	(+0.0013)	(+0.0023)
$[Xe]5d^{9}6s^{1}6p^{1}$	−0.9476	−0.4843	−0.1733	0.6547
	(−0.0055)	(+0.0011)	(+0.0011)	(+0.0021)
$[Xe]5d^{9}6s^{0}6p^{2}$	−1.0444	−0.5455	−0.2175	0.9743
	(−0.0062)	(+0.0008)	(+0.0011)	(+0.0022)
$[Xe]5d^{10}6s^{0}6p^{0}$	−1.1870	−0.8104	−0.4696	0.5666
	(+0.0033)	(−0.0008)	(−0.0011)	(−0.0006)

(*d*) Configuration	Valence state eigenvalues (Ryd) d	s	p	Excitation energy (Ryd)
$[Xe]5d^{10}6s^{1}6p^{0}$	−0.5300	−0.4514	−0.0718	0
	(+0.0039)	(+0.0008)	(+0.0032)	(0)
$[Xe]5d^{10}6s^{0}6p^{1}$	−0.6785	−0.5636	−0.1541	0.3930
	(+0.0028)	(−0.0001)	(+0.0029)	(+0.0028)
$[Xe]5d^{9}6s^{2}6p^{0}$	−0.6838	−0.5139	−0.0976	0.1232
	(+0.0001)	(+0.0022)	(+0.0049)	(+0.0007)
$[Xe]5d^{9}6s^{1}6p^{1}$	−0.8283	−0.6200	−0.1738	0.5535
	(−0.0020)	(+0.0009)	(+0.0046)	(+0.0025)
$[Xe]5d^{9}6s^{0}6p^{2}$	−0.9502	−0.7049	−0.2289	1.0149
	(−0.0035)	(+0.0005)	(+0.0049)	(+0.0066)
$[Xe]5d^{10}6s^{0}6p^{0}$	−1.1515	−1.0022	−0.5146	0.7218
	(+0.0052)	(−0.0001)	(−0.0032)	(−0.0004)

Atomic ground state configurations and their total energies are given in table 2. The total energies for the all-electron atoms, E^{ae}_{atom}, are obtained by non-relativistic spin-polarised calculations or fully relativistic calculations including spin–orbit coupling. For the total energies of the pseudo-atoms, E^{ps}_{atom}, the difference between the spin-polarised and the non-spin-polarised non-relativistic all-electron energies has been added to the energy obtained from the non-spin-polarised pseudo-atom calculation to take spin-polarisation into account.

The radial parts of the atomic valence pseudo-wavefunctions are shown in figure 1. As already expected from the eigenvalues of table 1, the effect of relativity is small for the 4d elements, but for the 5d elements the s and p pseudo-wavefunctions are clearly shifted towards the nuclei and the d pseudo-wavefunctions are pulled outside. This, together with the shifts of the s and p eigenvalues to lower and the d eigenvalues to higher energies, is an indication of the relativistic contraction of s and p core orbitals (Christensen 1984). The s and p valence wavefunctions are indirectly attracted by the core due to the condition that valence states have to be orthogonal to core states. The repulsion of the d wavefunctions is caused by the fact that the nuclear potential is more

Table 2. (*a*) Non-relativistic atomic ground state configurations and total energies. (*b*) Scalar-relativistic atomic ground state configurations and total energies. The experimental data for the ground state configurations are taken from Ashcroft and Mermin (1976). (ae: all-electron calculation; ps: pseudopotential calculations.)

(*a*) Element	Ground state (calculation)	E^{ae}_{atom} (Ryd)	E^{ps}_{atom} (Ryd)	Ground state (experiment)
Rh	$[Kr]4d^9$	−9366.4124	−44.6355	$[Kr]4d^85s^1$
Pd	$[Kr]4d^{10}$	−9870.4142	−58.6979	$[Kr]4d^{10}$
Ag	$[Kr]4d^{10}5s^1$	−10 389.7416	−74.9122	$[Kr]4d^{10}5s^1$
Ir	$[Xe]5d^9$	−33 602.8898	−41.1184	$[Xe]5d^76s^2$
Pt	$[Xe]5d^{10}$	−34 652.4919	−53.5467	$[Xe]5d^96s^1$
Au	$[Xe]5d^{10}6s^1$	−35 720.7484	−67.7138	$[Xe]5d^{10}6s^1$

(*b*) Element	Ground state (calculation)	E^{ae}_{atom} (Ryd)	E^{ps}_{atom} (Ryd)	Ground state (experiment)
Rh	$[Kr]4d^9$	−9548.6836	−44.1501	$[Kr]4d^85s^1$
Pd	$[Kr]4d^{10}$	−10 071.2594	−58.0775	$[Kr]4d^{10}$
Ag	$[Kr]4d^{10}5s^1$	−10 610.6253	−74.2067	$[Kr]4d^{10}5s^1$
Ir	$[Xe]5d^86s^1$	−35 623.7294	−40.2402	$[Xe]5d^76s^2$
Pt	$[Xe]5d^{10}$	−36 797.4073	−52.3990	$[Xe]5d^96s^1$
Au	$[Xe]5d^{10}6s^1$	−37 996.1895	−66.5306	$[Xe]5d^{10}6s^1$

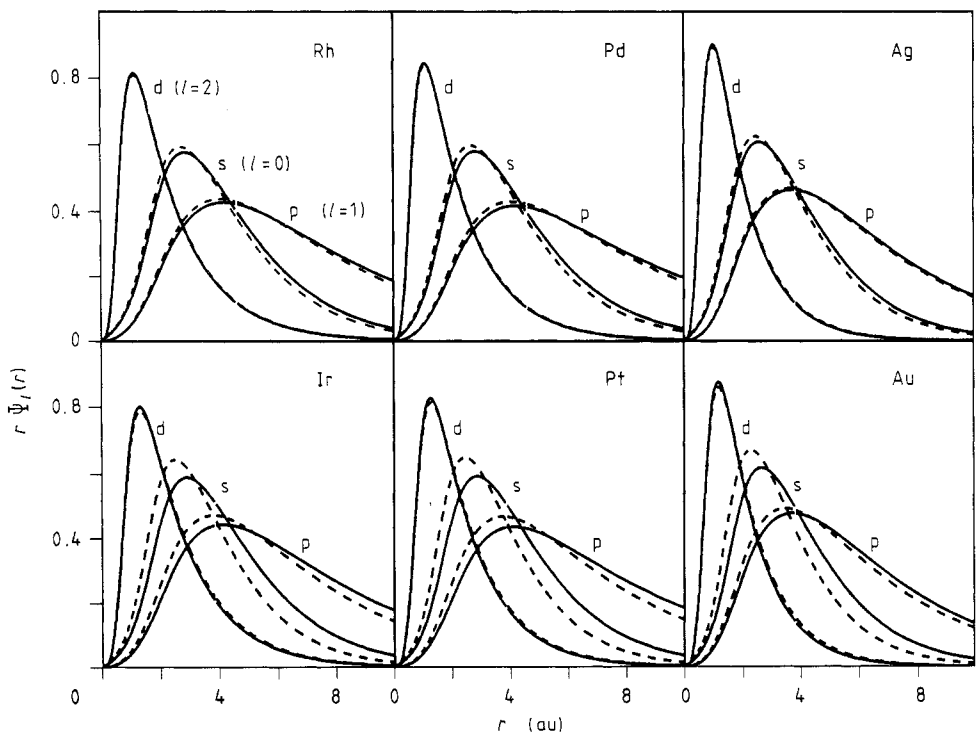

Figure 1. Radial parts of pseudo wave functions of the atomic valence orbitals; full curve: non-relativistic calculations; broken curve: scalar-relativistic calculations (1 au = 0.529 Å).

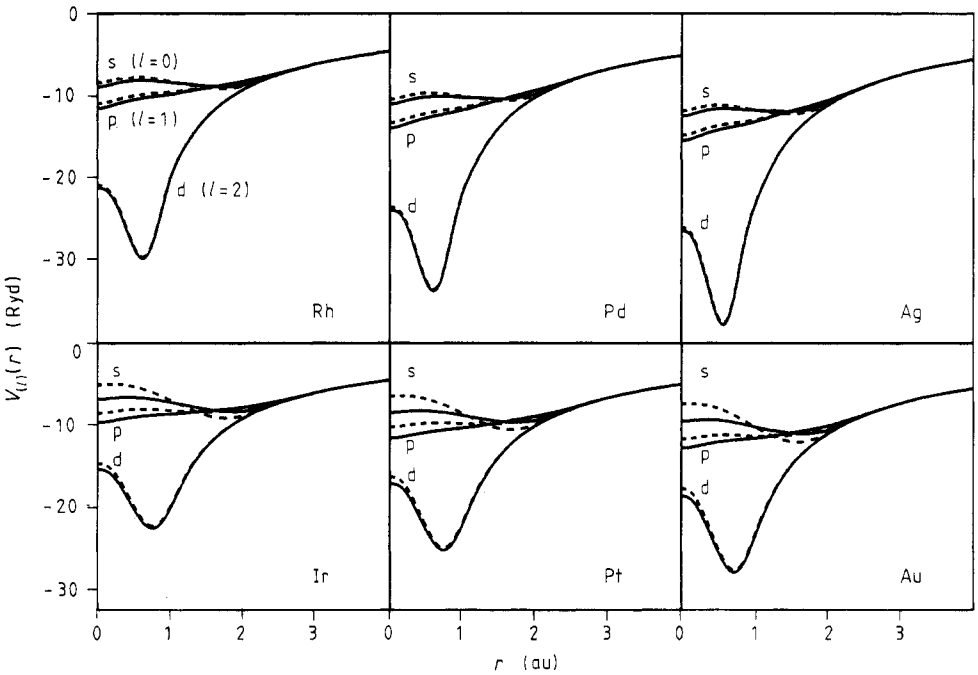

Figure 2. Radial parts of the angular-momentum-dependent ionic pseudopotentials; full curve: non-relativistic calculations; broken curve: scalar-relativistic calculations (1 au = 0.529 Å, 1 Ryd = 13.606 eV).

strongly screened by the higher density of the contracted core charge around the nucleus. In the scheme used by us these changes in the valence states due to the relativistic cores are correctly simulated by the relativistic pseudopotentials.

In figure 2 the radial parts of the non-relativistic and scalar-relativistic ionic pseudopotentials are shown for the six elements. We notice again that for the three 4d elements the differences are very small, whereas for the 5d elements there are bigger changes. As already mentioned, close to the heavy nucleus the relativistic potentials are weaker due to the increased screening. The s and p potentials are screened more strongly than the d potentials which could lead to the conclusion that the s and p wavefunctions should be shifted away from the nucleus even more than the d wavefunctions. However, here the orthogonality constraint to the contracted deep core s and p states over-compensates the weakening of the potentials, whereas for the valence d orbitals no corresponding effect is operative because d core orbitals are not close enough to the nucleus to be contracted considerably.

2.2. Mixed basis

For our calculations of the electronic structure of the valence states in the solids we have used an energy-independent mixed-basis set (Louie *et al* 1979). It contains a moderate number of plane waves augmented by well localised functions centred at the atomic sites to describe the localised d states. Since the earlier publication (Louie *et al* 1979) several improvements, which will be outlined in this section, have been incorporated.

In the mixed-basis method the wavefunctions for a crystal with several atoms per unit cell are given by

$$\psi_{nk}(\boldsymbol{r}) = \left(\sum_{\boldsymbol{G}} \alpha_{\boldsymbol{G}}^{nk} \frac{1}{\sqrt{\Omega}} e^{i(\boldsymbol{k}+\boldsymbol{G})\cdot\boldsymbol{r}} + \sum_{j,l,m} \beta_{jlm}^{nk} \phi_{jlm}^{k}(\boldsymbol{r})\right). \tag{1}$$

$\{\alpha_{\boldsymbol{G}}^{nk}\}$ and $\{\beta_{jlm}^{nk}\}$ are the elements of the eigenvector matrix $\boldsymbol{\Lambda}$ of the Hamiltonian matrix $\mathbf{H}$,

$$(1/\sqrt{\Omega})\, e^{i(\boldsymbol{k}+\boldsymbol{G})\cdot\boldsymbol{r}} \tag{2}$$

are the plane waves and $\phi_{jlm}^{k}(\boldsymbol{r})$ are Bloch sums

$$\phi_{jlm}^{k}(\boldsymbol{r}) = \frac{1}{\sqrt{N}} \sum_{\boldsymbol{R}} e^{i\boldsymbol{k}\cdot(\boldsymbol{R}+\boldsymbol{r}_j)}\, \varphi_{lm}(\boldsymbol{r} - \boldsymbol{R} - \boldsymbol{r}_j) \tag{3}$$

of localised basis functions centred at the positions of atomic nuclei in the crystal ($\boldsymbol{r}' = \boldsymbol{r} - \boldsymbol{R} - \boldsymbol{r}_j$):

$$\varphi_{lm}(\boldsymbol{r}') = i^l f_l(r') K_{lm}(\hat{\boldsymbol{r}}') \qquad r' = |\boldsymbol{r}'| \qquad \hat{\boldsymbol{r}}' = \boldsymbol{r}'/|\boldsymbol{r}'|. \tag{4}$$

The $f_l(r')$ are for example Gaussians or, in our case, numerical functions described below. The cubic harmonics $K_{lm}(\hat{\boldsymbol{r}}')$ are given by

$$\left.\begin{matrix} K_{l,+m}(\vartheta, \varphi) \\ K_{l,-m}(\vartheta, \varphi) \end{matrix}\right\} = \sqrt{\frac{2l+1}{2\pi(1+\delta_{0,m})} \frac{(l-m)!}{(l+m)!}} (-1)^m P_l^m(\cos\vartheta) \begin{cases} \cos m\varphi \\ \sin m\varphi \end{cases} \tag{5}$$

with $m = 0, 1, \ldots, l$, containing associated Legendre polynomials $P_l^m(\cos\vartheta)$ as given by Abramowitz and Stegun (1965). Ω is the volume of the whole crystal containing N unit cells with volumes Ω_C. $\boldsymbol{R}$ are the lattice translation vectors and $\boldsymbol{r}_j$ is the basis vector of the j^{th} atom in a lattice unit cell. It is convenient to include the factor i^l in (4) in order to get real Fourier transforms of the localised functions (see (13) below).

Localised d-like numerical functions $f_l(r)$ have been derived from atomic valence d pseudo-wavefunctions $\psi_l(r)$ ($l = 2$; see figure 1) by cutting off the tails beyond a certain radius r_c. A smooth decay to zero at r_c is created by multiplying with a cut-off function:

$$f_l(r) = \begin{cases} (1/\sqrt{C})\psi_l(r)\{1 - \exp[-\alpha(r_c - r)^2]\} & \text{for } r \leqslant r_c \\ 0 & \text{for } r > r_c. \end{cases} \tag{6}$$

C is a normalisation constant ($\int_0^\infty r^2 f_l^2(r)\, dr = 1$), α is a parameter determined variationally. The cut-off radii have been chosen close to the experimentally observed nearest-neighbour distances: Rh/Ir: $r_c = 2.55$ au; Pd/Pt: $r_c = 2.6$ au; Ag/Au: $r_c = 2.7$ au. The number of plane waves required for the completeness of the mixed basis is minimal, if the spheres containing the localised basis functions approximately touch each others.

The number of plane waves is given by a cut-off energy, $E_c = |\boldsymbol{k} + \boldsymbol{G}|^2$. For all six elements we have found that $E_c = 10.5$ Ryd, corresponding to about 60–70 plane waves per atom, has been sufficient to converge the total energy to 10^{-3} Ryd, if the localised basis functions have been carefully optimised. This optimisation has been done by varying the parameter α of equation (6) for fixed r_c and E_c to get a minimum for the total energy. In all cases we have found $\alpha = 0.7$ to be the best value. The basis parameters for the non-relativistic and the scalar-relativistic cases have turned out to be equal

because the d states are only weakly affected by relativity. Even for the elements in the same column of the periodic system (Rh/Ir, Pd/Pt, Ag/Au) the same parameters have been found to be optimal.

For the calculation of the overlap matrix **S** and the Hamiltonian matrix **H** matrix elements containing both plane waves (equation (2)) and Bloch sums of the localised functions (equation (3)) have to be evaluated.

In the original mixed-basis method each Bloch sum (equation (3)) is expanded in a Fourier series:

$$\phi^{k}_{jlm}(\boldsymbol{r}) = \sum_{\boldsymbol{G}} \phi_{jlm}(\boldsymbol{k}+\boldsymbol{G})(1/\sqrt{\Omega})\,\mathrm{e}^{\mathrm{i}(\boldsymbol{k}+\boldsymbol{G})\cdot\boldsymbol{r}}. \tag{7}$$

The periodicity volume is the unit cell volume Ω_C. The Fourier transform $\phi_{jlm}(\boldsymbol{k}+\boldsymbol{G})$ of the Bloch sum

$$\phi_{jlm}(\boldsymbol{k}+\boldsymbol{G}) = \frac{1}{\Omega}\int_{\Omega} \mathrm{e}^{-\mathrm{i}(\boldsymbol{k}+\boldsymbol{G})\cdot\boldsymbol{r}}\phi^{k}_{jlm}(\boldsymbol{r})\,\mathrm{d}^3r \tag{8}$$

can be written in the following form:

$$\phi_{jlm}(\boldsymbol{k}+\boldsymbol{G}) = \mathrm{e}^{-\mathrm{i}\boldsymbol{G}\cdot\boldsymbol{r}_j}\,\varphi_{lm}(\boldsymbol{k}+\boldsymbol{G}) \tag{9}$$

with the Fourier transform $\varphi_{lm}(\boldsymbol{k}+\boldsymbol{G})$ of the localised orbital of equation (4) (volume $\Omega \to \infty$)

$$\varphi_{lm}(\boldsymbol{k}+\boldsymbol{G}) = \frac{1}{\sqrt{\Omega_C}}\int_{\Omega} \mathrm{e}^{-\mathrm{i}(\boldsymbol{k}+\boldsymbol{G})\cdot\boldsymbol{r}}\varphi_{lm}(\boldsymbol{r})\,\mathrm{d}^3r \tag{10}$$

and the structure factor $\mathrm{e}^{-\mathrm{i}\boldsymbol{G}\cdot\boldsymbol{r}_j}$ of the j^{th} atom in the unit cell. Then the plane-wave expansion of the Bloch sums is finally given by

$$\phi^{k}_{jlm}(\boldsymbol{r}) = \sum_{\boldsymbol{G}} \mathrm{e}^{-\mathrm{i}\boldsymbol{G}\cdot\boldsymbol{r}_j}\varphi_{lm}(\boldsymbol{k}+\boldsymbol{G})\frac{1}{\sqrt{\Omega}}\mathrm{e}^{\mathrm{i}(\boldsymbol{k}+\boldsymbol{G})\cdot\boldsymbol{r}} \tag{11}$$

which renders possible the evaluation of all the matrix elements in Fourier space (Louie *et al* 1979, Zunger and Cohen 1979, Ihm *et al* 1979).

The plane-wave expansion of the Bloch sums (11) requires, because of their strongly localised nature, a much bigger number of plane waves than that used in the expansion of the crystalline wavefunction (equation (1)). Although the dimension of the Hamiltonian and overlap matrices is not increased, the necessary summations in the Fourier space consume a considerable amount of computing time, especially for the double sums in the local-orbital–local-orbital matrix elements.

A higher efficiency is possible by calculating all local-orbital–local-orbital and local-orbital–plane-wave matrix elements in real space. Instead of expanding the Bloch sums in the Fourier space (equation (11)) the plane waves are locally expanded in the real space:

$$\mathrm{e}^{\mathrm{i}\boldsymbol{q}\cdot\boldsymbol{r}} = \sum_{L=0}^{\infty}\sum_{M=-L}^{+L} 4\pi\mathrm{i}^{L}j_L(qr)K_{LM}(\hat{\boldsymbol{q}})K_{LM}(\hat{\boldsymbol{r}}) \tag{12}$$

in terms of spherical Bessel functions j_L (Abramowitz and Stegun 1965) and cubic harmonics K_{LM}. The three-dimensional integral in equation (10) is then given by ($\boldsymbol{q} = \boldsymbol{k}+\boldsymbol{G}$)

$$\varphi_{lm}(\boldsymbol{q}) = f_l(q)K_{lm}(\hat{\boldsymbol{q}}) \qquad q = |\boldsymbol{q}| \qquad \hat{\boldsymbol{q}} = \boldsymbol{q}/|\boldsymbol{q}| \tag{13}$$

with the one-dimensional integral

$$f_l(q) = \frac{1}{\sqrt{\Omega_C}} \int_0^\infty 4\pi r^2 j_l(qr) f_l(r)\, dr \tag{14}$$

and the cubic harmonic $K_{lm}(\hat{\boldsymbol{q}})$. With the numerical functions of equation (6) for the localised functions $f_l(r)$ the integrand vanishes for $r > r_c$.

The matrix elements of the overlap matrix are now given by

$$\begin{aligned}
&\langle \boldsymbol{k} + \boldsymbol{G}' | \boldsymbol{k} + \boldsymbol{G} \rangle = \delta_{\boldsymbol{G}',\boldsymbol{G}} \\
&\langle \phi^{\boldsymbol{k}}_{jlm} | \boldsymbol{k} + \boldsymbol{G} \rangle = e^{i\boldsymbol{G}\cdot\boldsymbol{r}_j} \varphi^*_{lm}(\boldsymbol{k} + \boldsymbol{G}) \\
&\langle \phi^{\boldsymbol{k}}_{jlm} | \phi^{\boldsymbol{k}}_{j'l'm'} \rangle = \delta_{j,j'} \delta_{l,l'} \delta_{m,m'}.
\end{aligned} \tag{15}$$

The 'on-site' expression in the last equation is an approximation if the integrand in equation (14) extends to infinity, for example for Gaussians, but it is exact for the numerical functions of equation (6) as long as the spheres around neighbouring sites do not overlap.

The Hamiltonian for the valence electrons consists of three parts, $H = T + V^{\mathrm{loc}} + V^{\mathrm{nl}}$. T is the kinetic energy, V^{loc} is the local part of the pseudopotential. V^{nl}, which is non-local in Fourier space, contains the angular-momentum-dependent contributions to the pseudopotential. (More details about the pseudopotential are given in appendix A.) The matrix of the kinetic energy has the following elements:

$$\begin{aligned}
&\langle \boldsymbol{k} + \boldsymbol{G}' | T | \boldsymbol{k} + \boldsymbol{G} \rangle = |\boldsymbol{k} + \boldsymbol{G}|^2 \delta_{\boldsymbol{G}',\boldsymbol{G}} \\
&\langle \phi^{\boldsymbol{k}}_{jlm} | T | \boldsymbol{k} + \boldsymbol{G} \rangle = |\boldsymbol{k} + \boldsymbol{G}|^2 \langle \phi^{\boldsymbol{k}}_{jlm} | \boldsymbol{k} + \boldsymbol{G} \rangle \langle \phi^{\boldsymbol{k}}_{jlm} | T | \phi^{\boldsymbol{k}}_{j'l'm'} \rangle \\
&\qquad = \int_0^{r_c} \left[\left(\frac{d}{dr} (r f_l(r)) \right)^2 + l(l+1) f_l^2(r) \right] dr\, \delta_{j,j'} \delta_{l,l'} \delta_{m,m'}.
\end{aligned} \tag{16}$$

The plane-wave–plane-wave matrix elements contain the main part of the non-spherical contributions of the potential in the interstitial regions. In the evaluation of the local-orbital–local-orbital and local-orbital–plane-wave matrix elements we assume that the potential is spherically symmetric within the range r_c around the atomic sites $\boldsymbol{r}_j$. Then the matrix elements of the local part are given by:

$$\begin{aligned}
&\langle \boldsymbol{k} + \boldsymbol{G}' | V^{\mathrm{loc}} | \boldsymbol{k} + \boldsymbol{G} \rangle = V^{\mathrm{loc}}(\boldsymbol{G}' - \boldsymbol{G}) \\
&\langle \phi^{\boldsymbol{k}}_{jlm} | V^{\mathrm{loc}} | \boldsymbol{k} + \boldsymbol{G} \rangle = \int_0^{r_c} r^2 f_l(r) V_j^{\mathrm{loc}}(r) j_l(|\boldsymbol{k} + \boldsymbol{G}| r)\, dr \left(\int_0^{r_c} r^2 f_l(r) j_l(|\boldsymbol{k} + \boldsymbol{G}| r)\, dr \right)^{-1} \\
&\qquad \times \langle \phi^{\boldsymbol{k}}_{jlm} | \boldsymbol{k} + \boldsymbol{G} \rangle \\
&\langle \phi^{\boldsymbol{k}}_{jlm} | V^{\mathrm{loc}} | \phi^{\boldsymbol{k}}_{j'l'm'} \rangle = \int_0^{r_c} r^2 f_l^2(r) V_j^{\mathrm{loc}}(r)\, dr\, \delta_{j,j'} \delta_{l,l'} \delta_{m,m'}.
\end{aligned} \tag{17}$$

The matrix elements of the non-local part are

$$\begin{aligned}
&\langle \boldsymbol{k} + \boldsymbol{G}' | V^{\mathrm{nl}} | \boldsymbol{k} + \boldsymbol{G} \rangle = V^{\mathrm{nl}}(\boldsymbol{k} + \boldsymbol{G}', \boldsymbol{k} + \boldsymbol{G}) \\
&\langle \phi^{\boldsymbol{k}}_{jlm} | V^{\mathrm{nl}} | \boldsymbol{k} + \boldsymbol{G} \rangle = \int_0^{r_c} r^2 f_l(r) \bar{V}_{(l)}(r) j_l(|\boldsymbol{k} + \boldsymbol{G}| r)\, dr \left(\int_0^{r_c} r^2 f_l(r) j_l(|\boldsymbol{k} + \boldsymbol{G}| r)\, dr \right)^{-1} \\
&\qquad \times \langle \phi^{\boldsymbol{k}}_{jlm} | \boldsymbol{k} + \boldsymbol{G} \rangle \\
&\langle \phi^{\boldsymbol{k}}_{jlm} | V^{\mathrm{nl}} | \phi^{\boldsymbol{k}}_{j'l'm'} \rangle = \int_0^{r_c} r^2 f_l^2(r) \bar{V}_{(l)}(r)\, dr\, \delta_{j,j'} \delta_{l,l'} \delta_{m,m'}.
\end{aligned} \tag{18}$$

The complete eigenvalue problem has the following form:

$$(\mathbf{H} - \mathbf{ES})\,\Lambda = \mathbf{0}. \tag{19}$$

E is a diagonal matrix containing the eigenvalues $\varepsilon_n(\boldsymbol{k})$ of **H**. The eigenvalue problem is transformed to standard form by Cholesky decomposition (Louie *et al* 1979) and then solved numerically at 60 different $\boldsymbol{k}$-points within the irreducible part of the first Brillouin zone (IBZ).

The charge density $\rho(\boldsymbol{r})$ of the valence electrons is given by

$$\rho(\boldsymbol{r}) = \sum_{n,k} w_{nk} |\psi_{nk}(\boldsymbol{r})|^2. \tag{20}$$

The w_{nk} are weighting factors which contain the weights of the $\boldsymbol{k}$-points in the IBZ and the occupations of the one-electron Bloch states $\psi_{nk}(\boldsymbol{r})$ (equation (2)). The occupations are determined by a Gaussian-smearing method (Fu and Ho 1983).

In former publications using mixed-basis representations (e.g. Fu and Ho 1983, Takeuchi *et al* 1989) only the Bloch wavefunctions were represented by the mixed basis (equation (2)). The charge density was expanded in a Fourier series, i.e. by a pure plane-wave basis set:

$$\rho(\boldsymbol{r}) = \sum_{G} \rho(\boldsymbol{G}) \mathrm{e}^{\mathrm{i}\boldsymbol{G}\cdot\boldsymbol{r}}. \tag{21}$$

The number of plane waves for this expansion had to be much bigger than that used in equation (2).

Recently we have developed a mixed-basis scheme for the representation of the charge density in real space, $\rho(\boldsymbol{r})$:

$$\rho(\boldsymbol{r}) = \sum_{n,k} w_{nk} \left| \sum_{G} \alpha_G^{nk} \frac{1}{\sqrt{\Omega}} \mathrm{e}^{\mathrm{i}(k+G)\cdot r} + \sum_{j,l,m} \beta_{jlm}^{nk} \phi_{jlm}^{k}(\boldsymbol{r}) \right|^2 \tag{22}$$

$$\rho(\boldsymbol{r}) = \rho^{(0)}(\boldsymbol{r}) + \rho^{(1)}(\boldsymbol{r}) + \rho^{(2)}(\boldsymbol{r}). \tag{23}$$

The first term, $\rho^{(0)}(\boldsymbol{r})$, is extended over the whole space and contains the pure plane-wave part of $\rho(\boldsymbol{r})$:

$$\rho^{(0)}(\boldsymbol{r}) = \sum_{n,k} w_{nk} \left| \sum_{G} \alpha_G^{nk} \frac{1}{\sqrt{\Omega}} \mathrm{e}^{\mathrm{i}(k+G)\cdot r} \right|^2 = \frac{1}{\Omega_C} \sum_{G,G'} \left(\frac{1}{N} \sum_{n,k} w_{nk} (\alpha_G^{nk})^* \alpha_{G'}^{nk} \right) \mathrm{e}^{\mathrm{i}(G'-G)\cdot r}. \tag{24}$$

It can be evaluated, as earlier, by Fourier transformation:

$$\rho^{(0)}(\boldsymbol{r}) = \sum_{G} \rho^{(0)}(\boldsymbol{G})\, \mathrm{e}^{\mathrm{i}\boldsymbol{G}\cdot\boldsymbol{r}} \tag{25}$$

with

$$\rho^{(0)}(\boldsymbol{G}) = \frac{1}{\Omega_C} \int_{\Omega_C} \mathrm{e}^{-\mathrm{i}\boldsymbol{G}\cdot\boldsymbol{r}} \rho^{(0)}(\boldsymbol{r})\, \mathrm{d}^3 r = \sum_{G'} \frac{1}{N} \sum_{n,k} w_{nk} (\alpha_{G'-G}^{nk})^* \alpha_{G'}^{nk} \tag{26}$$

but now, because the localised parts are not contained, a much smaller number of plane waves is sufficient.

The second and the third term contain the pure local orbital part, $\rho^{(1)}(\boldsymbol{r})$, and the mixed local-orbital–plane-wave part, $\rho^{(2)}(\boldsymbol{r})$, of $\rho(\boldsymbol{r})$:

$$\rho^{(1)}(\boldsymbol{r}) = \sum_{n,k} w_{nk} \left| \sum_{j,l,m} \beta_{jlm}^{nk} \phi_{jlm}^{k}(\boldsymbol{r}) \right|^2 \tag{27}$$

$$\rho^{(2)}(\boldsymbol{r}) = \sum_{n,k} w_{nk} 2 \,\mathrm{Re}\left(\sum_{G,j,l,m} \alpha_G^{nk} (\beta_{jlm}^{nk})^* \frac{1}{\sqrt{\Omega}} \mathrm{e}^{\mathrm{i}(\boldsymbol{k}+\boldsymbol{G})\cdot\boldsymbol{r}} \phi_{jlm}^{k*}(\boldsymbol{r}) \right). \tag{28}$$

Because the functions $f_l(r')$ contained in $\phi_{jlm}^k(\boldsymbol{r})$ ((3) and (4)) vanish for $r > r_c$, these two terms only give contributions to the total charge within the spheres of radius r_c around the atomic positions.

After inserting the Bloch sums of the localised functions (equations (3) and (4)) and the local expansion of the plane waves (equation (12)) $\rho^{(1),(2)}$ are given by the lattice sums ($\boldsymbol{r}' = \boldsymbol{r} - \boldsymbol{R} - \boldsymbol{r}_j$):

$$\rho^{(1),(2)}(\boldsymbol{r}) = \sum_{\boldsymbol{R},j} \rho_j^{(1),(2)}(\boldsymbol{r} - \boldsymbol{R} - \boldsymbol{r}_j) \tag{29}$$

with

$$\rho_j^{(1)}(\boldsymbol{r}') = \sum_{l,l'} \sum_{m,m'} f_{l'}(r') f_l(r') K_{l'm'}(\hat{\boldsymbol{r}}') K_{lm}(\hat{\boldsymbol{r}}') \left(\mathrm{i}^{l'-l} \frac{1}{N} \sum_{nk} w_{nk} \beta_{jl'm'}^{nk} (\beta_{jlm}^{nk})^* \right) \tag{30}$$

and

$$\rho_j^{(2)}(\boldsymbol{r}') = \sum_{G,l,m} \frac{1}{N} \sum_{n,k} w_{nk} \sum_{L=0}^{\infty} \sum_{M=-L}^{+L} \frac{4\pi}{\sqrt{\Omega_C}} f_l(r') j_L(|\boldsymbol{k}+\boldsymbol{G}|r') K_{lm}(\hat{\boldsymbol{r}}') K_{LM}(\hat{\boldsymbol{r}}') K_{LM}(\boldsymbol{k}+\boldsymbol{G})$$
$$\times 2\mathrm{Re}[\mathrm{i}^{L-l} \mathrm{e}^{\mathrm{i}\boldsymbol{G}\cdot\boldsymbol{r}_j} \alpha_G^{nk} (\beta_{jlm}^{nk})^*]. \tag{31}$$

The lattice sums are evaluated via the Fourier transformation

$$\rho^{(1),(2)}(\boldsymbol{r}) = \sum_{G} \rho^{(1),(2)}(\boldsymbol{G}) \mathrm{e}^{\mathrm{i}\boldsymbol{G}\cdot\boldsymbol{r}} \tag{32}$$

with

$$\rho^{(1),(2)}(\boldsymbol{G}) = \frac{1}{\Omega_C} \int_{\Omega_C} \mathrm{e}^{-\mathrm{i}\boldsymbol{G}\cdot\boldsymbol{r}} \rho^{(1),(2)}(\boldsymbol{r}) \,\mathrm{d}^3 r = \sum_j \mathrm{e}^{-\mathrm{i}\boldsymbol{G}\cdot\boldsymbol{r}_j} \sum_{\mathscr{L}=0}^{\infty} \sum_{\mathscr{M}=-\mathscr{L}}^{+\mathscr{L}} 4\pi \mathrm{i}^{-\mathscr{L}} K_{\mathscr{L}\mathscr{M}}(\hat{\boldsymbol{G}})$$
$$\times \int_{\Omega} \rho_j^{(1),(2)}(\boldsymbol{r}) j_{\mathscr{L}}(Gr) K_{\mathscr{L}\mathscr{M}}(\hat{\boldsymbol{r}}) \,\mathrm{d}^3 r. \tag{33}$$

The angle-dependent parts of the three-dimensional integrals are given by Gaunt coefficients (Condon and Shortley 1935, Tinkham 1964). The radial parts are integrated numerically. The angular momentum expansion in equation (31) has been carried out until $L = 4$.

The total charge density of the valence electrons in Fourier space, which will be used for the total-energy calculation (Ihm *et al* 1979), is given by the sum of the densities obtained from equations (26) and (33). According to equations (23), (25) and (32), the total charge density in real space can be obtained now by fast Fourier transformation (FFT) (see, for example, Press *et al* 1986). Since in equation (20) the summation is done only over the $\boldsymbol{k}$-points within the IBZ, the charge density finally needs to be symmetrised (see appendix B).

2.3. *Total energies and cohesive properties*

We have calculated total energies for the solids using the Fourier space formalism of Ihm *et al* (1979) with charge densities determined according to the aforementioned prescription.

Sufficient self-consistency is achieved if the change in the total energy between two iteration steps is less than 10^{-5} Ryd. Then the differences in the Fourier components of the input and output potentials are less than 10^{-4} Ryd.

To get the cohesive properties we have calculated total energies for eight to ten different values of Wigner–Seitz cell volumes in a range of about (10–20)% around the equilibrium volume. The ground state energies of the free atoms, $E_{\text{atom}}^{\text{ps}}$, have been chosen as a reference for the total energies (see table 2).

An analytic function for the energy–volume curve has been fitted to the data (Rose *et al* 1981). This universal binding curve is characterised by three quantities, the equilibrium atomic volume V_0 in the solid, the cohesive energy $E_0 = E(V_0)$ and the bulk modulus $B_0 = V_0 \, \mathrm{d}^2E/\mathrm{d}V^2|_{V_0}$:

$$E(V) = E_0(1 + \sigma)\, \mathrm{e}^{-\sigma} \tag{34}$$

where $\sigma = (s - s_0)/\lambda$ is a dimensionless length quantity, s and s_0 are atomic sphere radii ($V = (4\pi/3)s^3$, $V_0 = (4\pi/3)s_0^3$) and the length parameter λ is given by:

$$\lambda = [1/(36\pi V_0^3)^{1/3}]\sqrt{-E_0 V_0/B_0}. \tag{35}$$

3. Cohesive properties

The energy–volume curves, from which we have extracted the cohesive properties of the considered FCC transition metals, are presented in figure 3. To be able to use the same axis scales for all elements we have set the zero level of the ordinates at the energy minima. For comparison we have included universal binding curves corresponding to experimental data for V_0, B_0 and E_0 (Kittel 1975).

Our calculated equilibrium lattice constants $a_0 = (4V_0)^{1/3}$, bulk moduli B_0 and cohesive energies E_0 are listed in the first rows of tables 3, 4 and 5, respectively, together with values from experiment (last row) and other calculations.

Figure 3 shows much bigger differences between the non-relativistic and the scalar-relativistic energy–volume curves for the 5d than for the 4d elements. This fact is demonstrated more clearly in figure 4, where the calculated ground state quantities are compared with experimental values. For the 5d metals the scalar-relativistic equilibrium volumes and bulk moduli are significantly closer to the experiment than the non-relativistic ones. This fact seems to be very reasonable because the atomic nuclei of the 5d elements are already heavy enough to cause sizable relativistic effects, as shown above by the results of the atomic calculations. The agreement of the scalar-relativistic results for all three quantities with the experiment is not perfect, but it is in the range commonly accepted for results of the LDA for transition metals. The non-relativistic equilibrium volumes and bulk moduli, on the other hand, deviate much more from experiment. Relativistic effects on core electrons near the nuclei and their indirect influence on the valence electrons via the orthogonality condition and screening effects for the wave functions contained in the pseudopotential are not negligible for 5d metals.

In the case of the 4d metals the agreement of the scalar-relativistic results with experiment is as good as for the 5d metals. The non-relativistic values are in some cases even closer to the experiment than the scalar-relativistic ones. This behaviour is unexpected because for the core electrons the non-relativistic treatment (Hamann *et al* 1979) is more approximate than the scalar-relativistic treatment (Bachelet and Schlüter 1982).

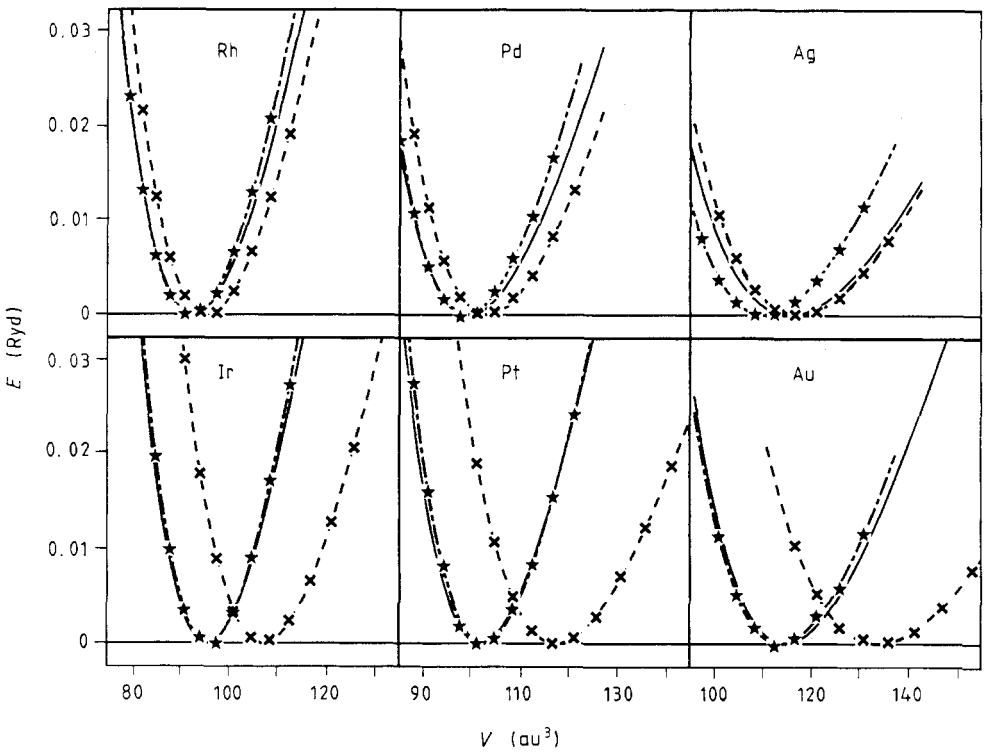

Figure 3. Calculated total energies (dots) and fitted universal binding curves; the zero level of the ordinates goes through the minima of the fit-curves; full curve: fit-curves to experimental data (Kittel 1975); broken curve with crosses: non-relativistic calculations; chain curve with stars: scalar-relativistic calculations ($1\,(\text{au})^3 = 0.148\,\text{Å}^3$, 1 Ryd = 13.606 eV).

Comparing our results for the 4d metals with others (compare tables 3, 4 and 5) we find a nearly perfect agreement of our non-relativistic data with those of the non-relativistic calculations of Moruzzi *et al* (1978). Our scalar-relativistic values for the 4d and the 5d metals are also in good agreement with nearly all other available scalar-relativistic calculations (Jepsen 1989, Methfessel and Kübler 1982, Terakura *et al* 1987, Wei *et al* 1987). Therefore the somewhat higher quality of non-relativistic over scalar-relativistic data for the 4d metals is not an artifact of the mixed-basis pseudopotential method we have used, but some kind of error cancellation effect within the LDA.

We find the non-relativistic bulk modulus and cohesive energy of each 5d element to be nearly equal to those of its corresponding 4d element (see tables 4 and 5 and figure 4). Only the lattice constant is bigger, because of the larger core.

Which rules of thumb can we use to assess the degree of precision with which scalar-relativistically cohesive properties of transition metals are calculated (the ranges of our values are given in brackets below)? The lattice constants are very close to the experimental values ($-1.5\% < \Delta a_0/a_0 < +0.3\%$) while the bulk moduli and cohesive energies are always overestimated ($+5.1\% < \Delta B_0/B_0 < +26.1\%$, $+3.9\% < \Delta|E_0|/|E_0| < +39.0\%$).

For the 4d metals, using the non-relativistic approach, lattice constants are slightly bigger than experimental values ($+0.5 < \Delta a_0/a_0 < +1.3\%$) while bulk moduli and

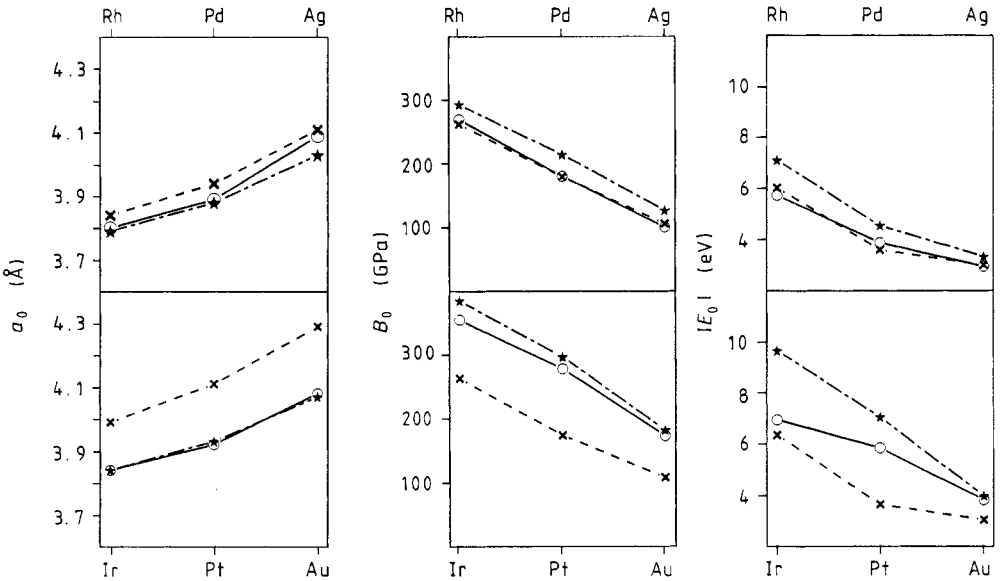

Figure 4. Lattice constants a_0, bulk moduli B_0 and cohesive energies $|E_0|$ for the 4d metals (upper panels) and 5d metals (lower panels). The data points are connected by straight lines to accentuate the trends; full curve with circles: experimental data (Kittel 1975); broken curve with crosses: non-relativistic data (MB); chain curve with stars: scalar-relativistic data (MB).

cohesive energies show no unique trend ($-2.7\% < \Delta B_0/B_0 < +5.3\%$, $-7.2\% < \Delta|E_0|/|E_0| < +5.2\%$).

Comparing the non-relativistic and the scalar-relativistic results we find that relativistic effects reduce the equilibrium volumes and increase bulk moduli and cohesive energies (compare figure 4).

4. Electronic structures

In this section we give a description of the changes appearing in the valence charge densities and band structures due to relativistic effects. We confine ourselves to the presentation of the electronic structure of Pt which shows all the effects also seen in Ir and Au and, to a lesser extent, in Rh, Pd and Ag.

In figure 5 non-relativistic and scalar-relativistic band structures along symmetry lines of the irreducible part of the first Brillouin zone are plotted. Splittings of degeneracies due to spin–orbit coupling in fully relativistic band structures (Christensen 1984) are of minor importance for the ground state properties considered here because the centres of energy of the multiplets coincide with the scalar-relativistic levels and mostly the levels of one multiplet and all either occupied or empty. Figure 5(*a*) shows the non-relativistic band structure at the equilibrium volume (117 au^3). The other parts of figure 5 show scalar-relativistic band structures at three different volumes: (*b*) non-relativistic equilibrium volume (117 au^3); (*c*) scalar-relativistic equilibrium volume (101 au^3); (*d*) compressed volume (91 au^3) at which the total energy has increased again to approximately the value in figure 5(*b*) (compare figure 4).

Table 3. Lattice constants a_0 for the (*a*) 4d and (*b*) 5d metals (in Å); references: [1] Takeuchi *et al* (1989), [2] Moruzzi *et al* (1978), [3] Jepsen (1989) (*d*) [4] Williams *et al* (1979), [5] Methfessel and Kübler (1982), [6] Terakura *et al* (1987), [7] Wei *et al* (1987) and [8] Kittel (1975). In contrast to the present contribution the charge densities in reference [1] are still represented by a pure plane-wave basis set (see Louie *et al* 1979) and not yet by a mixed basis. For silver both Gaussians and numerical functions have been used for the localised basis functions (Gaussian/numerical function).

(*a*)	Rhodium		Palladium		Silver		
Method	NR	SR	NR	SR	NR	SR	Reference
MB	3.84	3.79	3.94	3.88	4.11	4.03	
MB					4.108/4.115		[1]
KKR	3.83		3.93		4.12		[2]
LMTO		3.714		3.788		3.934	[3]
ASW	3.86		3.91		4.13		[4]
ASW				3.866			[5]
ASW						4.028	[6]
LAPW						4.057	[7]
Exp.	3.80		3.89		4.09		[8]
(*b*)	Iridium		Platinum		Gold		
Method	NR	SR	NR	SR	NR	SR	Reference
MB	3.99	3.84	4.11	3.93	4.29	4.07	
MB					4.314	4.104	[1]
LMTO		3.764		3.835		3.986	[3]
ASW		3.851		3.921		4.057	[5]
ASW						4.070	[6]
LAPW						4.106	[7]
Exp.	3.84		3.92		4.08		[8]

Table 4. Bulk moduli B_0 for the (*a*) 4d and (*b*) 5d metals (in GPa); references as for table 3.

(*a*)	Rhodium		Palladium		Silver		
Method	NR	SR	NR	SR	NR	SR	Reference
MB	263	294	180	215	106	127	
MB					108.0/96.1		[1]
KKR	261		170		102		[2]
ASW						137	[6]
LAPW						106	[7]
Exp.	270.4		180.8		100.7		[8]
(*b*)	Iridium		Platinum		Gold		
Method	NR	SR	NR	SR	NR	SR	Reference
MB	263	385	174	297	108	182	
MB					99.6	179.0	[1]
ASW						189	[6]
LAPW						180	[7]
Exp.	355.0		278.3		173.2		[8]

Table 5. Cohesive energies $|E_0|$ for the (*a*) 4d and (*b*) 5d metals (in eV); references: as for table 3.

(*a*)	Rhodium		Palladium		Silver		
Method	NR	SR	NR	SR	NR	SR	Reference
MB	6.05	7.14	3.61	4.56	3.01	3.34	
MB					2.64/3.01		[1]
KKR	6.11		3.69		2.88		[2]
LAPW						3.53	[7]
Exp.	5.75		3.89		2.95		[8]
(*b*)	Iridium		Platinum		Gold		
Method	NR	SR	NR	SR	NR	SR	Reference
MB	6.34	9.65	3.64	7.05	3.03	3.96	
MB					2.27	3.46	[1]
LAPW						4.35	[7]
Exp.	6.94		5.84		3.81		[8]

In the comparison of the non-relativistic and the scalar-relativistic band-structure for the same unit-cell volume (5(*a*) and (*b*)) there are two most obvious changes due to relativity. First at the Fermi surface one big hole structure of the highest band along Γ–L nearly vanishes and another one along Γ–X becomes smaller. The Fermi surface is modified by relativistic effects. The second change is a shift of the lowest band away from the second lowest band. Both changes can be understood as a shift of the s band to lower energies relative to the d bands. For example the pure d states $\Gamma_{25'}$ and Γ_{12} at the Γ point in the centre of the first Brillouin zone retain the same energies relative to the Fermi energy as in the non-relativistic bands, only the s state Γ_1 is shifted down considerably. This relative shift between d and s bands causes an increased overlap of their densities of states which allows for an increase in the s–d hybridisation.

With the reduction of the unit-cell volume (figure 5(*c*) and (*d*)) the relativistic bands remain qualitatively unchanged; but now the s and d bands become broader indicating an increased electronic pressure due to the higher average charge density.

For an illustration of changes in the valence charge density of the crystal and a discussion of the chemical bonding we have found it convenient to subtract a superposition of spherically symmetric charge densities of free atoms located at the lattice sites from the charge density in the solid:

$$\Delta\rho(\boldsymbol{r}) = \rho^{\text{solid}}(\boldsymbol{r}) - \sum_{\boldsymbol{R},j} \rho_j^{\text{atom}}(\boldsymbol{r} - \boldsymbol{R} - \boldsymbol{r}_j). \tag{36}$$

For the free Pt atoms we have used the spherically symmetric charge density of the closed shell configuration [Xe]$5d^{10}$ which is our calculated atomic ground state configuration (compare tables 2(*a*) and 2(*b*)).

Contour plots of the charge density differences $\Delta\rho(\boldsymbol{r})$ in a {100} and a {111} plane are shown in figures 6 and 7. The density difference plotted in each panel of both figures belongs to the same calculation as the band structure shown in the corresponding panel of figure 5. In table 6 we give values for the density differences $\Delta\rho(\boldsymbol{r})$ at special locations in the crystal.

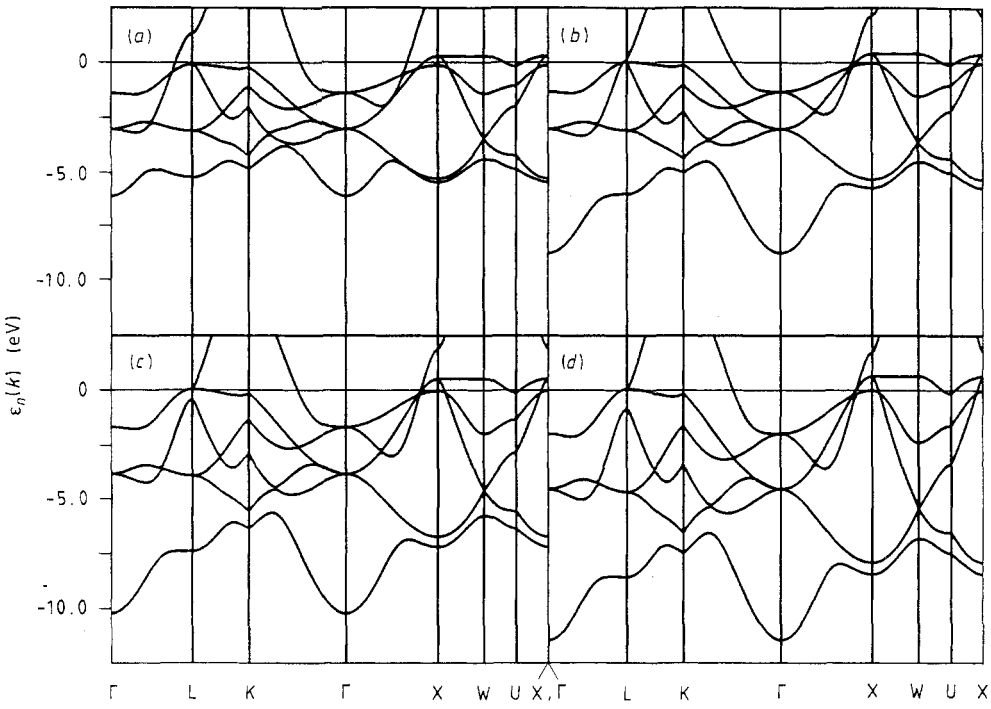

Figure 5. Band structures of Pt along symmetry lines of the irreducible part of the first Brillouin zone; the Fermi energy has been set as the zero level. (*a*) non-relativistic calculation, $V = V_0^{nr} = 117(\text{au})^3$; (*b*) scalar-relativistic calculation, $V = 117(\text{au})^3$; (*c*) scalar-relativistic calculation, $V = V_0^{sr} = 101(\text{au})^3$; (*d*) scalar-relativistic calculation, $V = 91(\text{au})^3$.

Looking first at the non-relativistic cases (*a*) we see that the charge density in the interstitial regions of the solid is bigger than the superposed atomic densities illustrating the effect of chemical bonding. The reason for the increase of the density in the bonding regions and the decrease around the cores is mainly a s–d hybridisation of full d states with empty s states. In the {100} plane the density along the nearest-neighbour connection lines is higher than in the remaining interstitial region. This might suggest the existence of directed bonds in the transition metal. But in the {111} plane the whole interstitial region contains a nearly homogeneous charge distribution due to the close packing of the atoms in the FCC crystals.

Switching on relativity now by going from parts (*a*) to parts (*b*) we observe an increase of density between the nearest neighbours along the ⟨110⟩ directions. The reason for that is the increase of s–d hybridisation already indicated in the band structures.

The additional negative charge between the positively charged cores reduces their mutual electrostatic repulsion force. Furthermore, due to the contracted cores the electronic pressure of occupied s states can be reduced. The crystal prefers to assume a smaller volume (panels (*c*)). This relativistic equilibrium volume is again characterised by a homogeneous charge density in the whole interstitial region of the {111} plane of about the same amount as there already is along the ⟨110⟩ directions in panels (*b*). By a further compression below the relativistic equilibrium volume (panels (*d*)) the charge density along the ⟨110⟩ directions does not change. The density is only increased around the tetrahedral interstitial sites, located near the triangular interstitial regions of the

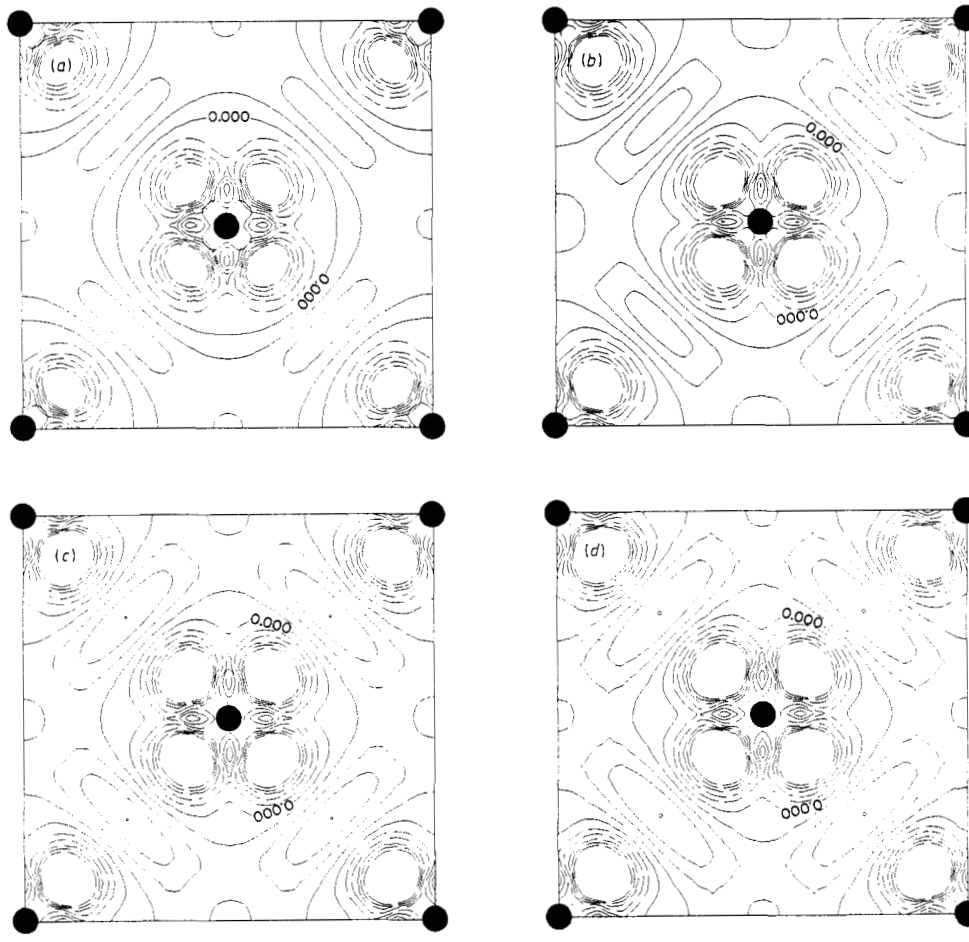

Figure 6. Contour plots for differences $\Delta\rho(\boldsymbol{r})$ in the charge density of the solid and the superposed charge densities of free atoms in the {100} planes of Pt. The atomic positions are indicated by black dots. Full curves indicate positive differences, broken curves negative differences. The unit for the densities is electrons au^{-3}. The interval between two contour lines is 2.5×10^{-3} electrons au^{-3}. Negative differences below -1.25×10^{-2} electrons au^{-3} near atomic sites have been cut off. For an explanation of the four panels see the caption of figure 5.

{111} plane. On the other hand, in the much bigger interstitial region around octahedral sites, located in the middle of the cube edges of the {100} planes, the density is much less sensitive to volume changes.

Concluding this section we have found that the equilibrium volume of the FCC transition metals is characterised by nearly the same charge density between neighbouring atoms and in tetrahedral interstitial regions originating from s–d hybridisation. By compression or dilation of the volume only the density in the interstitial regions is increased or reduced, respectively. The density around the atomic connection line is nearly not affected. The difference between the non-relativistic and scalar-relativistic results is an increased bonding charge density due to a higher s–d hybridisation. This causes a weakening of the core–core repulsion and therefore a reduction of the equilibrium volume.

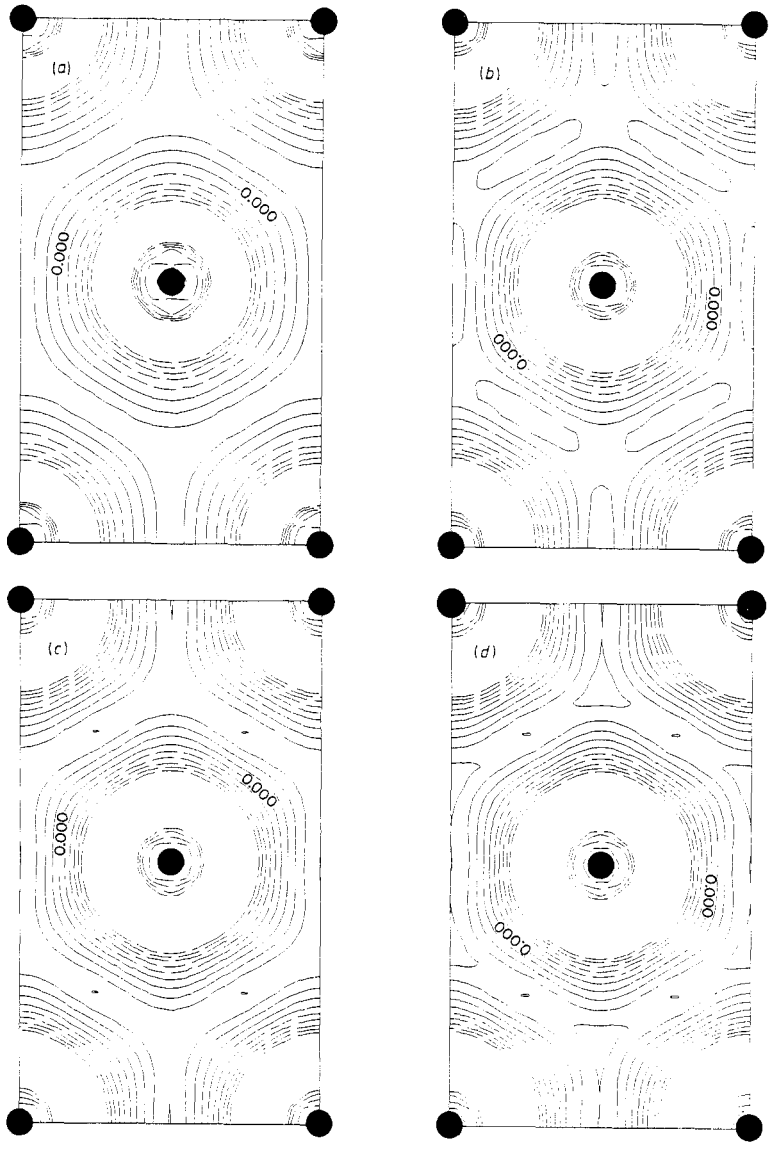

Figure 7. Contour plots for differences $\Delta\rho(r)$ in the {111} planes of Pt. For an explanation see the captions of figures 5 and 6.

As well as the reduction of the volume due to relativity, we have seen in section 3 that both the relativistic bulk moduli and cohesive energies are larger than the non-relativistic ones (compare tables 4, 5 and figure 4). The larger bulk moduli are closely connected with the smaller volumes. Moruzzi *et al* (1978) have shown that the bulk modulus depends approximately on the average charge density (corresponding to a homogeneous free-electron charge density) within the Wigner–Seitz cell, rather than on the actual inhomogenous density. In the relativistic crystal, due to the reduced volume, the increased average charge density yields the larger bulk modulus. The reason for the bigger relativistic cohesive energies is the gain of bonding energy in the solid due to the stronger s–d hybridisation.

Table 6. Charge density differences $\Delta\rho(r)$ at special locations in the contour plots of the figures 6 and 7 (in 10^{-3} electrons au^{-3}; bond.: bonding region in the middle between two nearest-neighbour atoms, oct.: octahedral interstitial region in the {100} plane, tri.: triangular interstitial region in the {111} plane; for explanation of panels (*a*)–(*d*) see caption of figure 6.

Panel	(*a*)	(*b*)	(*c*)	(*d*)
bond.	6.7	9.4	10.1	10.1
oct.	2.5	2.1	2.1	2.2
tri.	5.9	7.2	9.2	10.8

5. Summary

In this article we have presented a comparative investigation of the influence of relativity on the cohesive properties of 4d and 5d transition metals with face-centred cubic crystal structures.

We have used a first-principles pseudopotential method for total-energy calculations in a mixed-basis representation. Since an earlier contribution (Louie *et al* 1979) this method has been improved in several ways. The charge densities are now computed in real and Fourier space simultaneously, which increases the computational efficiency.

Our results for the transition metals are summarised as follows: for the 5d metals scalar-relativistic corrections have to be taken into account to get reasonable values for equilibrium volumes, bulk moduli and cohesive energies of the crystals.

For the 4d metals we have found that the results of the more approximate non-relativistic calculations are better than those of the presumably more accurate scalar-relativistic ones. We suppose that this behaviour is due to an error cancellation effect.

The differences in the cohesive properties have been related to the changes in the band structures and charge densities of the valence electrons. The main reason for the differences is an increase in the s–d hybridisation of the valence orbitals which is indirectly originated by the relativistic core contraction via the orthogonality constraint for all orbitals and the weakening of the ionic pseudopotentials.

Acknowledgments

The Ames Laboratory is operated for the US Department of Energy by the Iowa State University under contract No W-7405-Eng-82. The helpful information and comments from Dr O Jepsen and Dr N E Christensen are gratefully acknowledged. One of us (CE) would like to thank Professor Dr B N Harmon and Professor Dr K-M Ho as well as Professor Dr H Kronmüller and Dr M Fähnle for providing the opportunity to spend one year with the solid-state theory group of the Ames Laboratory.

Appendix A. Pseudopotentials in Fourier space and in real space

The angular momentum dependent ionic pseudopotential derived from atomic all-electron wave functions in real space

$$V^{\text{ion}}(\boldsymbol{r}) = \sum_{l=0}^{2} V_{(l)}(r)\hat{P}_l. \tag{A1}$$

The radial parts $V_{(l)}(r)$ are shown in figure 2. $\hat{P}_l$ is an angular-momentum projection operator.

For a crystal, according to Ihm *et al* (1979), the local ($l = 0$) and the angular-momentum-dependent ($l = 1, 2$, non-local) parts of the pseudopotential in Fourier space are given by

$$V^{\mathrm{loc}}(\boldsymbol{G}' - \boldsymbol{G}) = S(\boldsymbol{G}' - \boldsymbol{G})V_{(0)}(|\boldsymbol{G}' - \boldsymbol{G}|) + V_{\mathrm{H}}(\boldsymbol{G}' - \boldsymbol{G}) + V_{\mathrm{X}}(\boldsymbol{G}' - \boldsymbol{G}) + V_{\mathrm{C}}(\boldsymbol{G}' - \boldsymbol{G}) \tag{A2}$$

$$V^{\mathrm{nl}}(\boldsymbol{k} + \boldsymbol{G}', \boldsymbol{k} + \boldsymbol{G}) = S(\boldsymbol{G}' - \boldsymbol{G}) \sum_{L} \bar{V}_{(L)}(\boldsymbol{k} + \boldsymbol{G}', \boldsymbol{k} + \boldsymbol{G}) \tag{A3}$$

with the structure factor

$$S(\boldsymbol{q}) = \sum_{j} \mathrm{e}^{-\mathrm{i}\boldsymbol{q}\cdot\boldsymbol{r}_j} \tag{A4}$$

and the non-local form factors

$$\bar{V}_{(L)}(\boldsymbol{q}', \boldsymbol{q}) = \frac{4\pi}{\Omega_{\mathrm{C}}}(2L + 1)P_L(\hat{\boldsymbol{q}}' \cdot \hat{\boldsymbol{q}}) \int_0^\infty \bar{V}_{(L)}(r) j_L(q'r) j_L(qr) r^2 \, \mathrm{d}r. \tag{A5}$$

The P_L are Legendre polynomials, the j_L are spherical Bessel functions (Abramowitz and Stegun 1965).

The local part of the pseudopotential contains all interactions with long range. In real space inside the sphere of radius r_c, centred at the site j, it is given by the Fourier transform

$$V_j^{\mathrm{loc}}(\boldsymbol{r}) = \sum_{\boldsymbol{G}} V^{\mathrm{loc}}(\boldsymbol{G}) \, \mathrm{e}^{\mathrm{i}\boldsymbol{G}\cdot\boldsymbol{r}_j} \mathrm{e}^{\mathrm{i}\boldsymbol{G}\cdot\boldsymbol{r}}. \tag{A6}$$

Using the local expansion for $\mathrm{e}^{\mathrm{i}\boldsymbol{G}\cdot\boldsymbol{r}}$ (equation (12)) and making the spherical approximation ($L = 0$ only) we obtain

$$V_j^{\mathrm{loc}}(r) = \sum_{\boldsymbol{G}} V^{\mathrm{loc}}(\boldsymbol{G}) \, \mathrm{e}^{\mathrm{i}\boldsymbol{G}\cdot\boldsymbol{r}_j} j_0(Gr). \tag{A7}$$

The angular-momentum-dependent part in real space has a short range of interaction ($r < r_c$). It is given by the radial part of the ionic pseudopotential:

$$\bar{V}_{(l)}(r) = V_{(l)}(r) - V_{(0)}(r). \tag{A8}$$

Appendix B. Charge symmetrisation

Since the electronic wave functions are computed only for the $\boldsymbol{k}$-points inside the irreducible part of the Brillouin zone (IBZ), the charge density computed from

$$\rho(\boldsymbol{r}) = \sum_{\boldsymbol{k} \in \mathrm{IBZ}, n} w_{\boldsymbol{n}\boldsymbol{k}} |\psi_{\boldsymbol{n}\boldsymbol{k}}(\boldsymbol{r})|^2$$

needs to be symmetrised.

For $\rho^{(0)}(\boldsymbol{r})$, the part of the charge density constructed from the plane-wave part of the basis, it is convenient to perform the symmetrisation in the Fourier space, i.e. the Fourier components $\rho^{(0)}(\boldsymbol{G})$, as defined in equation (26), are symmetrised. If the space

group $\{S_\mu|\boldsymbol{t}_\mu\}$ has M elements, where S_μ are point-group operations and $\boldsymbol{t}_\mu$ are non-primitive translation vectors, then the symmetrised Fourier components are given by

$$\rho^{(0)}_{\mathrm{sym}}(\boldsymbol{G}) = \frac{1}{M}\sum_{\mu=1}^{M} \rho^{(0)}(S_\mu \boldsymbol{G})\, \mathrm{e}^{-\mathrm{i}(S_\mu \boldsymbol{G})\cdot \boldsymbol{t}_\mu}. \tag{B1}$$

For $\rho^{(1)}$ and $\rho^{(2)}$, which are only non-zero inside a sphere ($r < r_c$) centred at the atomic sites in the present formulation, it is more convenient to symmetrise directly in the real space. Following equation (29), we write the charge density as

$$\rho(\boldsymbol{r}) = \sum_j \rho_j(\boldsymbol{r} - \boldsymbol{r}_j) \tag{B2}$$

where the $\boldsymbol{r}_j$ are the atomic sites with local orbitals inside the unit cell. Note that we have dropped the lattice vector $\boldsymbol{R}$ from equation (29) since we only need to symmetrise the charge density inside one unit cell. The functional form of $\rho_j(\boldsymbol{r} - \boldsymbol{r}_j)$ can always be expressed as

$$\rho_j(\boldsymbol{r}') = \sum_{l,m} F^{r_j}_{lm}(r') K_{lm}(\hat{\boldsymbol{r}}'). \tag{B3}$$

$F^{r_j}_{lm}(r')$, the radial charge distribution centred at the site $\boldsymbol{r}_j$ corresponding to the angular momentum index (l, m), can be deduced from equations (30) and (31).

The symmetrised charge is then given by

$$\rho_{\mathrm{sym}}(\boldsymbol{r}) = \sum_j \tilde{\rho}_j(\boldsymbol{r} - \tilde{\boldsymbol{r}}_j) \tag{B4}$$

where

$$\tilde{\rho}_j(\boldsymbol{r}') = \sum_{l,m'} \tilde{F}^{\tilde{r}_j}_{lm'}(r') K_{lm'}(\hat{\boldsymbol{r}}') \tag{B5}$$

with

$$\tilde{F}^{\tilde{r}_j}_{lm'}(r') = \frac{1}{M}\sum_{\mu=1}^{M}\sum_{m=-l}^{l} F^{r_j}_{lm}(r') U_{mm'}(S_\mu). \tag{B6}$$

$\tilde{\boldsymbol{r}}_j$ and $\boldsymbol{r}_j$ are related by $\tilde{\boldsymbol{r}}_j = S_\mu \boldsymbol{r}_j - \boldsymbol{t}_\mu$, and $U_{mm'}$ are rotation matrices defined by

$$S_\mu K_{lm}(\hat{\boldsymbol{r}}') = \sum_{m'} U_{mm'}(S_\mu) K_{lm'}(\hat{\boldsymbol{r}}').$$

References

Abramowitz M and Stegun I A 1965 *Handbook of Mathematical Functions* (New York: Dover) pp 331, 435

Andersen O K 1975 *Phys. Rev.* B **12** 3060

Andersen O K 1984 *The Electronic Structure of Complex Systems* ed W Temmerman and P Phariseau (New York: Plenum) p 59

Andersen O K, Jepsen O and Glötzel D 1985 *Highlights of Condensed Matter Theory* ed F Bassani, F Fumi and M P Tosi (Amsterdam: North-Holland) p 11

Andersen O K, Jepsen O and Sob M 1987 *Electronic Band Structure and its Applications* ed M Youssouff (Berlin: Springer) p 1

Ashcroft N W and Mermin N D 1976 *Solid State Physics* (Philadelphia: Saunders) p 1

Bachelet G B and Schlüter M 1982 *Phys. Rev.* B **25** 2103

Callaway J and March N H 1984 *Solid State Physics* vol 38 (New York: Academic) p 136

Chen Y, Ho K M and Harmon B N 1988 *Phys. Rev.* B **37** 283
Christensen N E 1984 *Int. J. Quantum Chem.* **25** 233
Cohen M L and Heine V 1970 *Solid State Physics* vol 24 (New York: Academic) p 37
Condon E U and Shortley G A 1935 *Theory of Atomic Spectra* (Cambridge: Cambridge University Press) p 1
Feynman R P 1939 *Phys. Rev.* **56** 340
Fu C L and Ho K M 1983 *Phys. Rev.* B **28** 5480
Hamann D R, Schlüter M and Chiang C 1979 *Phys. Rev. Lett.* **43** 1494
Hedin L and Lundqvist B I 1971 *J. Phys. C: Solid State Phys.* **4** 2064
Hellmann H 1937 *Einführung in die Quantenchemie* (Leipzig: Deuticke) p 1
Herman F and Skillman S 1963 *Atomic Structure Calculations* (Englewood Cliffs, NJ: Prentice-Hall) p 1
Ho K M and Bohnen K P 1987 *Phys. Rev. Lett.* **59** 1833
Ho K M, Fu C L and Harmon B N 1983 *Phys. Rev.* B **28** 6687
—— 1984 *Phys. Rev.* B **29** 1575
Hohenberg P and Kohn W 1964 *Phys. Rev.* B **136** 864
Ihm J 1988 *Rep. Prog. Phys.* **51** 105
Ihm J, Zunger A and Cohen M L 1979 *J. Phys. C: Solid State Phys.* **12** 4409
Jepsen O 1989 private communication (see also Andersen *et al* (1985))
Kittel C 1975 *Introduction to Solid State Physics* (New York: Wiley) pp 38, 96, 143
Kleinman L 1980 *Phys. Rev.* B **21** 2630
Koelling D D 1981 *Rep. Prog. Phys.* **44** 139
Kohn W and Rostoker N 1954 *Phys. Rev.* **94** 1111
Kohn W and Sham L J 1965 *Phys. Rev.* **140** A1133
Kohn W and Vashishta P 1983 *Theory of the Inhomogenous Electron Gas* ed S Lundqvist and N H March (New York: Plenum) p 79
Korringa J 1947 *Physica* **13** 392
Lam P K and Cohen M 1981 *Phys. Rev.* B **24** 4224
Louie S G, Ho K M and Cohen M 1979 *Phys. Rev.* B **19** 1774
Methfessel M 1988 *Phys. Rev.* B **38** 1537
Methfessel M and Kübler J 1982 *J. Phys. F: Met. Phys.* **12** 141
Moruzzi V L, Janak J F and Williams A R 1978 *Calculated Electronic Properties of Metals* (New York: Pergamon) p 1
Phillips J C and Kleinman L 1959 *Phys. Rev.* **116** 287
Press W H, Flannery B P, Teukolsky S A and Vetterling W T 1986 *Numerical Recipes* (Cambridge: Cambridge University Press) p 381
Rose J H, Ferrante J and Smith J R 1981 *Phys. Rev. Lett.* **47** 675
Skriver H R 1984 *The LMTO Method* (Berlin: Springer) p 1
Slater J C 1937 *Phys. Rev.* **51** 846
Takeuchi N, Chan C T and Ho K M 1989 *Phys. Rev.* B **40** 1565
Terakura K, Oguchi T, Mohri T and Watanabe K 1987 *Phys. Rev.* B **35** 2169
Tinkham M 1964 *Group Theory and Quantum Mechanics* (New York: McGraw-Hill) p 1
Wei S H, Mbaye A A, Ferreira L G and Zunger A 1987 *Phys. Rev.* B **36** 4163
Weinert M, Wimmer E and Freeman A J 1982 *Phys. Rev.* B **26** 4571
Weyrich K H 1988 *Phys. Rev.* B **37** 10269
Williams A R, Kübler J and Gelatt C D 1979 *Phys. Rev.* B **19** 6094
Wimmer E, Krakauer H, Weinert M and Freeman A J 1981 *Phys. Rev.* B **24** 864
Yin M T and Cohen M 1982 *Phys. Rev.* B **26** 5668
Zunger A and Cohen M 1979 *Phys. Rev.* B **19** 568